Oncogene (2005) 24, 6689–6698

www.nature.com/onc

Nitric oxide upregulates the cyclooxygenase-2 expression through the cAMP-response element in its promoter in several cancer cell lines

Seok-Woo Park[1,2], Myung-Whun Sung*[,1,2,3,4], Dae-Seog Heo[2,4,5], Hiroyasu Inoue[6], Seon-Hui Shim[2] and Kwang-Hyun Kim[3,4]

[1]*Department of Tumor Biology, College of Medicine, Seoul National University, 28, Yongun-dong, Chongno-gu, Seoul, Korea;* [2]*Cancer Research Institute, College of Medicine, Seoul National University, 28, Yongun-dong, Chongno-gu, Seoul, Korea;* [3]*Department of Otorhinolaryngology – Head and Neck Surgery, College of Medicine, Seoul National University, 28, Yongun-dong, Chongno-gu, Seoul, Korea;* [4]*Clinical Research Institute, College of Medicine, Seoul National University, 28, Yongun-dong, Chongno-gu, Seoul, Korea;* [5]*Department of Internal Medicine, College of Medicine, Seoul National University, 28, Yongun-dong, Chongno-gu, Seoul, Korea;* [6]*Department of Food Science and Nutrition, Nara Women's University, Nara, Japan*

We previously showed that nitric oxide (NO) induces overexpression of cyclooxygenase-2 (COX-2) and production of prostaglandin E_2 in cancer cells. Here, we investigated the mechanisms by which NO induces COX-2 expression in cancer cells. We found that the cAMP-response element (CRE) is a critical factor in NO-induced COX-2 expression in all cells tested. We found that in cancer cells, three transcription factors (TFs) – cAMP response element-binding protein (CREB), activating transcription factor-2 (ATF-2) and c-jun, bound the CRE in the COX-2 promoter, and their activities were increased by addition of the NO donor, *S*-nitroso-*N*-acetyl-D,L-penicillamine (SNAP). NO-induced activation of soluble guanylate cyclase (sGC), p38 and c-Jun NH_2-terminal kinase (JNK) upregulated the three TFs, leading to COX-2 overexpression. Addition of dibutyryl-cGMP (db-cGMP) induced COX-2 expression in a manner similar to SNAP; this induction was blocked by a p38 inhibitor (SB202190), but not by a JNK inhibitor (SP600125). NO-induced cGMP was found to activate CREB and ATF-2 in a p38, but not c-jun-dependent manner, while NO induced JNK in a cGMP-independent manner, leading to subsequent activation of c-jun and ATF-2. These results suggest that the low concentrations of endogenous NO present in cancer cell may induce the expression of many genes, including COX-2, which promotes the growth and survival of tumor cells.
Oncogene (2005) **24**, 6689–6698. doi:10.1038/sj.onc.1208816; published online 20 June 2005

Keywords: nitric oxide; NO; cyclooxygenase-2; COX-2; cAMP-response element; CRE

*Correspondence: M-W Sung, Department of Otorhinolaryngology – Head and Neck Surgery and Cancer Research Institute, Seoul National University College of Medicine, 28, Yongon-Dong, Chongno-Gu, Seoul 110-744, Korea; E-mail: mwsung@snu.ac.kr
Received 11 May 2004; revised 19 April 2005; accepted 2 May 2005; published online 20 June 2005

Introduction

In recent years, nitric oxide (NO) has been recognized as a fundamental signaling molecule for the maintenance of homeostasis, a potent cytotoxic effector molecule involved in the pathogenesis of a wide range of human diseases (Liaudet *et al.*, 2000). NO is also an important mediator of inflammatory responses, prompting researchers to investigate whether NO interacts with another inflammatory factor, cyclooxygenase-2 (COX-2), in inflammatory cells. Previous reports showed that when inducible NO synthase (iNOS) was upregulated in inflammatory cells, COX-2 expression increased in a similar pattern (Surh *et al.*, 2001). NO has been reported to activate or inhibit COX-2 activity, depending on the concentration of NO, the timing of its induction, and the investigated cell type (Salvemini *et al.*, 1993; Stadler *et al.*, 1993; Tsai *et al.*, 1994; Habib *et al.*, 1997).

It is well known that iNOS and COX-2 are simultaneously upregulated in various cancers, including head and neck cancer (Gallo *et al.*, 1998; Chan *et al.*, 1999; Son *et al.*, 2001; Lee *et al.*, 2002; Nose *et al.*, 2002). However, the direct cross-talk between NO and COX-2 in cancer cells has not been fully elucidated. Recently, we showed that NO induces COX-2 expression and prostaglandin E_2 (PGE_2) production in head and neck cancer cells, and that this effect is blocked by iNOS inhibitors. Similar results have been shown in other cancer cells, including hepatocarcinoma, gastric cancer and cervical cancer (Park *et al.*, 2003).

The role of NO in cancer is unclear and somewhat controversial, but may be divided into two broad functions: promotion of cancer progression and/or cytotoxicity to cancer cells. At high concentrations, NO acts as a tumoricidal factor, though it can also initiate tumorigenesis through genotoxic mutations. At lower (noncytotoxic) levels, NO has been reported to promote cancer progression during invasion, metastasis and angiogenesis (Gallo *et al.*, 1998; Wink *et al.*, 1998; Surh *et al.*, 2001). In cancer cells, COX-2 is known

to facilitate malignant progression though various mechanisms (Sheng *et al.*, 2001; Pai *et al.*, 2002; Sun *et al.*, 2002; Tanabe and Tohnai, 2002). COX-2 is one of the immediate early response genes; its expression is regulated by trans-activation of a regulatory signal leading to activation of specific transcription factors (TFs) that subsequently bind regulatory sites in the COX-2 promoter. NF-κB, NF-IL6, PEA-3 and cAMP response element-binding protein (CREB)/activator protein-1 (AP-1) have been suggested to play important roles in the regulation of the COX-2 expression in various cells; their response elements have been located close to the transcription initiation site of the COX-2 promoter (Howe *et al.*, 2001; Tang *et al.*, 2001; Tamura *et al.*, 2002; Tanabe and Tohnai, 2002). NO affects the activity of many TFs in various pathways. NO transduces intracellular signaling through the activation of sGC, which is the only receptor conclusively proven to mediate interactions between NO and its signaling molecules (Bogdan, 2001). However, it is not yet known how COX-2 expression is upregulated by endogenous NO in cancer cells, or whether NO plays an important role in carcinogenesis.

Here, we investigated the mechanisms of NO-induced overexpression of COX-2 by analysing the action of NO on signals related to the regulation of COX-2 expression in cancer cells. We found that NO increases COX-2 expression through the cAMP response element (CRE) of the COX-2 promoter in cancer cells. The data suggest that the low concentrations of endogenous NO present in cancer cells may induce the expressions of diverse genes, such as COX-2, which promotes the growth and survival of tumor cells.

Results

CRE is an important transcription regulatory element for basal and NO-induced COX-2 expression in SNU-1041 cells

We performed luciferase assays with plasmids containing partial COX-2 promoter sequences (−1432/+59(L), −327/+59(S), KBM, CRM, ILM, KBM+CRM, KBM+ILM, CRM+ILM and Triple M) (Figure 1b) and observed that the CRE was a critical regulatory motif for basal and NO-induced overexpression of COX-2 in SNU-1041 cells. Basal luciferase activities were significantly lower in cells transfected with plasmids containing mutant CRE (CRM, CRM+KBM, CRM+ILM and Triple M) versus those with other plasmids (−327/+59(S), KBM, ILM and KBM+ILM) (Figure 1a). Similarly, cells transfected with plasmids harboring mutant CRE sequences showed significantly lower inductions of luciferase activity in response to the NO donors, phorbol 13-myristate 12-acetate (PMA) or *S*-nitroso-*N*-acetyl-D, L-penicillamine (SNAP) (Figure 1b). These data indicate that CRE is a critical regulatory motif for NO-induced COX-2 expression.

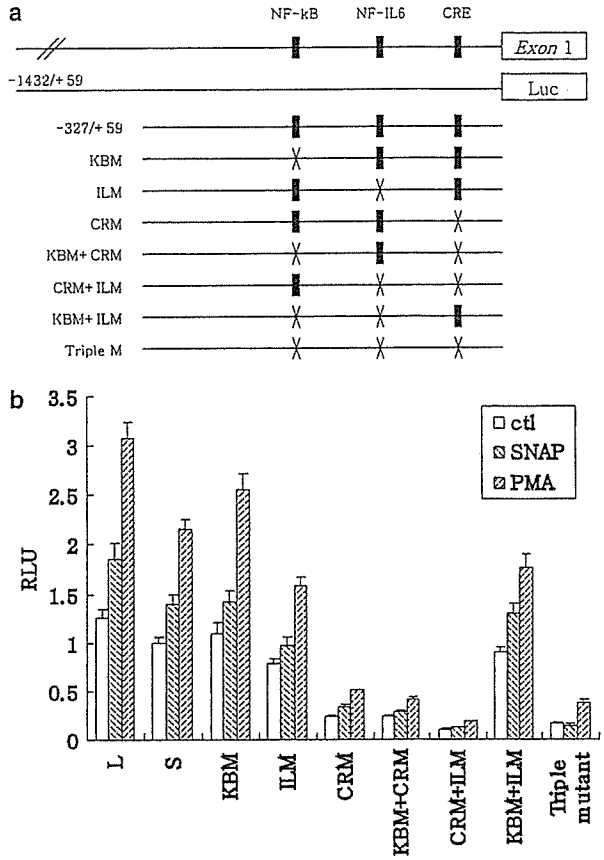

Figure 1 CRE is an important transcription regulatory element for basal and NO-induced COX-2 expression in SNU-1041 cells. (a) Schematic of the 5′-regulatory region of the human COX-2 gene and the utilized mutant constructs. Transcription factor binding sequences (■) and mutated sites (X) are indicated. (b) SNU-1041 cells were transfected with 0.5 μg of plasmids containing partial COX-2 promoters (−1432/+59(L), −327/+59(S), KBM, CRM, ILM, KBM+CRM, KBM+ILM, CRM+ILM and Triple M) and subsequently treated with 500 μM SNAP or 10 nM PMA for 18 h. Total cell lysates were prepared and COX-2 promoter activities were determined. Luciferase activity was normalized in relation to cotransfection with 0.5 μg pSV-β galactosidase control vector, and is presented in relative luciferase units (RLUs). Vertical bars indicate the standard deviation (s.d.)

CREB, activating transcription factor-2 (ATF-2) and c-jun bind to the CRE of the COX-2 promoter in SNU-1041 cells

To identify TFs that interact with the CRE of the COX-2 promoter, we performed a gel shift assay using four representative members of the CREB/ATF-2/AP-1 family of TFs: CREB, ATF-2, c-jun and c-fos (Figure 2a). Treated with antibody to CREB, ATF-2 and c-jun antibodies, but not by the anti-c-fos antibody, the decrease and dragged shift of the binding bands were detected in repeated experiments. Addition of unlabeled competitors against the CREB and AP-1 elements also decreased the intensity of the bands, while addition of an unlabeled competitor for NF-κB (cold control) did not. These results indicate that at least three of them

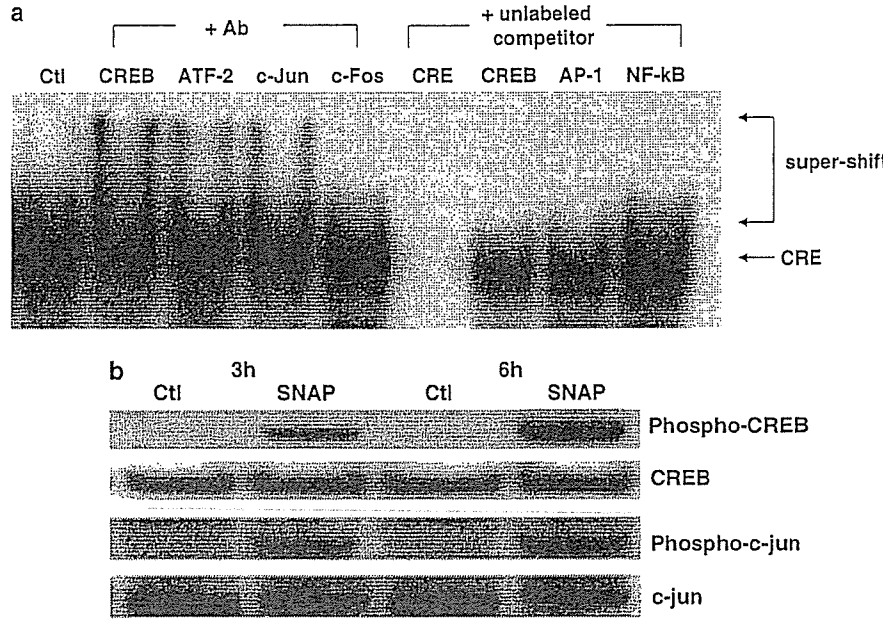

Figure 2 CREB, ATF-2 and c-jun bind to the CRE of the COX-2 promoter, and NO increases their activities in SNU-1041 cells. (a) Nuclear proteins (5 μg) were incubated with ^{32}P-labeled oligonucleotides containing the CRE site of COX-2, and 2 μl antibody and 1 μl unlabeled oligonucleotide competitors (25 ×) were added for competition assays. The unlabeled competitor for NF-κB was used as a cold control. (b) For Western blotting, cells were treated with 500 μM SNAP for 3 or 6 h. Total cellular proteins were extracted, 40 μg was loaded per lane, and the resulting immunoblots were probed for with antibodies against phospho-CREB, phospho-c-jun, CREB and c-jun

(CREB, ATF-2 and c-jun) control COX-2 expression by binding to the CRE of the COX-2 promoter.

NO phosphorylates and activates CREB, ATF-2 and c-jun in SNU-1041 cells

We next used the PathDetect Trans-Reporting system (Stratagene, La Jolla) to examine whether NO is capable of activating CREB, ATF-2 and/or c-jun. We found that NO treatment increased the activities of these TFs by 2- to 2.5-fold (Figures 4c and 5a). Western blotting revealed that CREB and c-jun were phosphorylated in cells treated with NO for 4–12 h (Figure 2b). These data indicate that NO activates the tested TFs via phosphorylation, providing a convincing link between NO and increased COX-2 expression.

NO-induced COX-2 expression is mediated partially through the cGMP-dependent pathway

As NO has been reported to control cellular signaling and gene expression through both cGMP-dependent (via activation of sGC) and -independent means (Bogdan, 2001), we examined whether cGMP is an upstream regulator of NO-induced COX-2 expression. SNU-1041 cells were treated with dibutyryl-cGMP (db-cGMP) for 18 h and their COX-2 expression was examined. The COX-2 expression in cells treated with db-cGMP was comparable to that in SNAP-treated cells (Figure 3a), and SNAP-induced COX-2 expression was inhibited by the NO-sensitive sGC inhibitor, 1H-[1,2,4]oxadiazolo[4,3,-a]quinoxalin-1-one (ODQ)

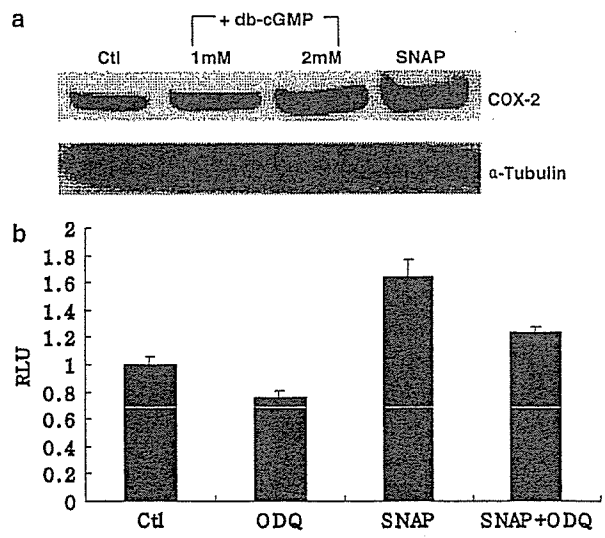

Figure 3 NO-induced COX-2 expression is mediated, in part, via the cGMP-dependent pathway in SNU-1041 cells. (a) Cells were treated with 1 or 2 mM dibutyryl-cGMP (db-cGMP) for 18 h and total cellular proteins (40 μg) were separated and transferred for Western blotting with an anti-COX-2 antibody. (b) Cells harboring the COX-2 promoter (−1432/+59) containing plasmid were incubated with 50 μM ODQ, 500 μM SNAP or 500 μM SNAP + 50 μM ODQ for 18 h and COX-2 expression was analysed in terms of luciferase activity normalized against that of β-galactosidase. The results presented are representative of three independent experiments, with the vertical bars representing the s.d.

(Figure 3b). These observations suggest that NO activates sGC to induce cGMP, leading to signals aimed at regulating COX-2 expression.

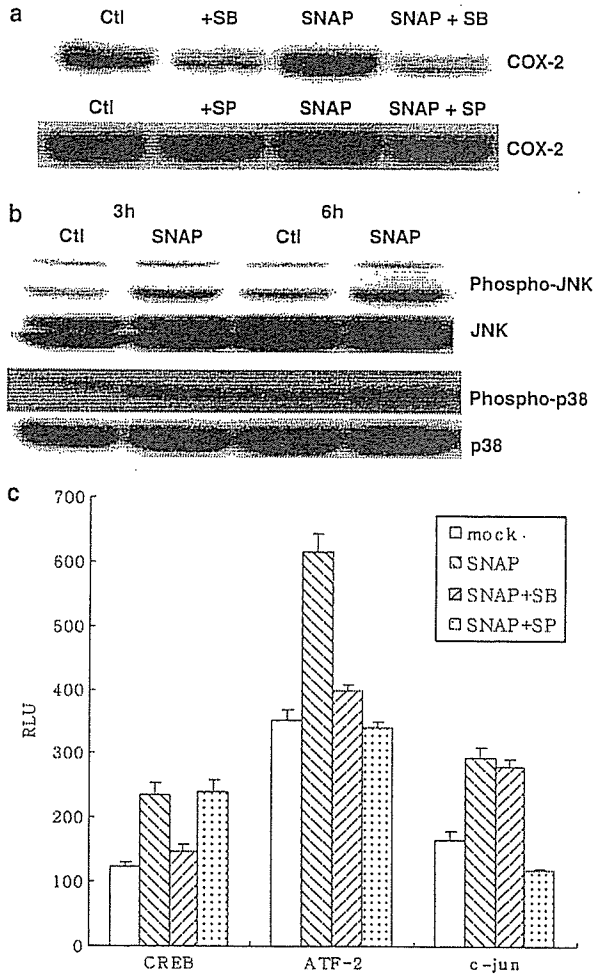

Figure 4 NO induces COX-2 expression via activation of p38 and JNK. (a) Cells were treated with 12.5 μM SB202190 (p38 MAPK inhibitor) or 10 μM SP600125 (JNK inhibitor) in the presence or absence of 500 μM SNAP for 18 h. Total proteins were extracted and 40 μg per lane was resolved, blotted and subjected to Western blotting with antibodies against COX-2. (b) Cells were treated with 500 μM SNAP for 2 or 4 h, and 40 μg of total protein was resolved and immunoblotted with antibodies against phospho-JNK, JNK, phospho-p38 and p38. (c) Cells transfected with 0.05 μg of pFA-ATF-2, pFA2-CREB, or pFA2-cJun were treated with 500 μM SNAP, 500 μM SNAP + 12.5 μM SB202190 or 500 μM SNAP + 10 μM SP600125 for 18 h, cell lysates were prepared, and RLUs was measured. Luciferase activity was normalized in relation to that of β-galactosidase. The vertical bars represent the s.d.

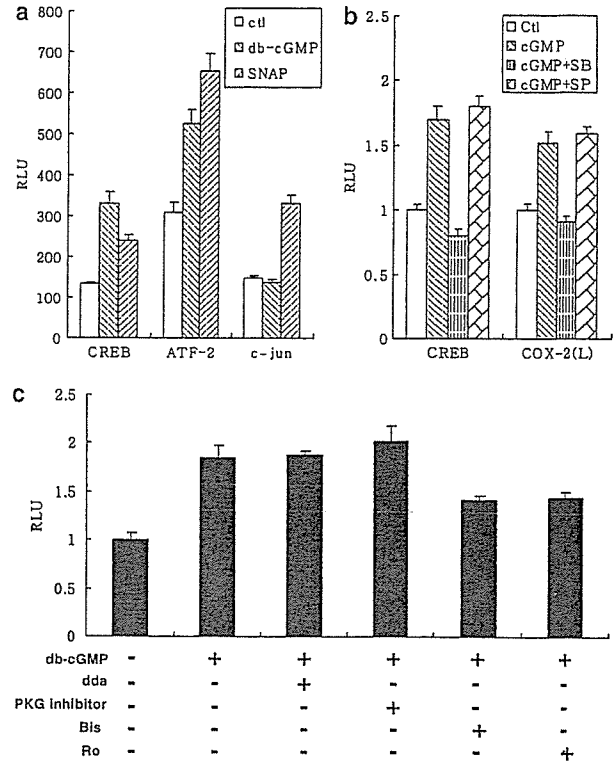

Figure 5 NO activation of p38 is cGMP-dependent, while that of JNK is cGMP-independent. Cells transfected with the indicated plasmids were treated for 18 h with (a) 2 mM db-cGMP or 500 μM SNAP, or (b) 2 mM db-cGMP, 2 mM db-cGMP + 12.5 μM SB202190, or 2 mM db-cGMP + 10 μM SP600125. (c) Cells transfected with pFA2-CREB were treated for 18 h with 2 mM db-cGMP, 2 mM db-cGMP + 200 μM 2-3-dda, 2 mM db-cGMP + 200 μM Rp-8-pCPT-cGMPs, 2 mM db-cGMP + 2 μM Bi-sindolylmaleimide I or 2 mM db-cGMP + 1 μM Ro-31-8220. Total cell lysates were extracted and RLUs were measured. Luciferase activities were normalized to that of β-galactosidase

NO induces COX-2 expression via activation of p38 and c-Jun NH_2-terminal kinase (JNK)

As three MAP kinases were known to be upstream regulators of COX-2 expression, we examined whether extracellular signal-regulated kinase (ERK), p38 and JNK were related to NO-induced COX-2 expression. NO-induced COX-2 expression was blocked by the p38 inhibitor, SB202190, and the JNK inhibitor, SP600125 (Figure 4a), but not by the ERK inhibitors, U0126 and PD153015 (data not shown). In addition, Western blotting revealed that the phosphorylation levels of p38 and JNK increased after 2–8 h of treatment with SNAP (Figure 4b), indicating that NO increased the phosphorylation of p38 and JNK. Furthermore, SB202190 treatment inhibited the NO-induced activation of CREB and ATF-2, while SP600125 treatment inhibited the NO-induced activation of ATF-2 and c-jun. These data indicate that among the CRE-associated TFs in the COX-2 promoter, CREB is activated by p38, c-jun is activated by JNK, and ATF-2 is activated by both (Figure 4c).

NO-induced activation of p38 is cGMP-dependent, while that of JNK is cGMP-independent

As we found that cGMP and two MAP kinases mediated NO-induced COX-2 expression, we examined whether there was any interaction between cGMP and MAP kinases in NO-induced COX-2 expression. Treatment of cells with db-cGMP upregulated the activity of

the p38 targets – CREB and ATF-2 – but not that of the JNK target – c-jun (Figure 5a). The db-cGMP-induced activities of CREB and the COX-2 promoter were blocked by the p38 inhibitor but not by the JNK inhibitor (Figure 5b). These data suggest that NO-induced cGMP upregulates p38 MAP kinase but not JNK. In an effort to identify the cGMP-activated upstream regulators of p38, we tested the effect of PKA, protein kinase-C (PKC), and protein kinase G (PKG) on cGMP-induced p38 activation. The PKC inhibitors (Bisindolylmaleimide I and Ro-31-8220) reduced the activation of p38 by ~30%, while inhibitors of PKA, PKG and Ca^{2+} had no detectable effects on the activation of p38 (Figure 5c). Thus, while we were unable to specifically define the regulators upstream of cGMP in this pathway, our results suggest some possible involvement of PKC.

The effect of NOS inhibitors on the activities of CREB and c-jun in SNU-1041 cells

To examine the effect of endogenous NO on the intracellular signaling pathways in cancer cells, we treated SNU-1041 cells with the universal NOS inhibitor, *N*-nitro-L-arginine-methyl ester (L-NAME), and the iNOS-specific inhibitors, 1400W and Aminoguanidine (AG), and examined their effects on the activities of CREB and c-jun. Treatment of cells with the NOS inhibitors inhibited the activities of CREB and c-jun (Figure 6). As NO-induced activation of these TFs is critical to the upregulation of COX-2 expression, these results suggest that COX-2 expression is likely to be decreased by blockage of NO production.

The effect of NO on COX-2 expression in other cancer cells

We previously observed that NO induces COX-2 overexpression in various cancer cells (Park *et al*., 2003). To investigate whether the NO-induced responses identified in this study are seen in cancer cells other than SNU-1041, we tested the effect of NO on another head and neck cancer cell line (PCI-13) and two cell lines originating from other cancer types (SNU-668 and HeLa). In PCI-13 and HeLa cells, the CRE was important for NO-induced COX-2 expression (Figure 7a), and this increase in COX-2 expression was blocked by the p38 inhibitor (Figure 7b and c). Furthermore, NO treatment upregulated the p38 targets, CREB and ATF-2, in these cells (Figure 7d, e). In SNU-668, COX-2 expression was increased by NO treatment, and this effect was partially reduced by p38 and JNK inhibitors (Figure 7c). Collectively, these observations indicate that NO upregulates COX-2 expression by activating p38 and/or JNK in diverse cancer cells.

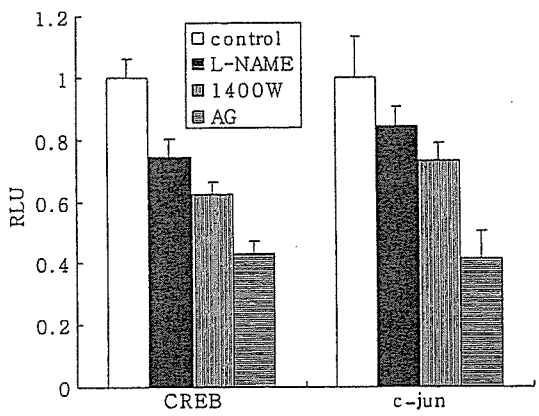

Figure 6 The effect of NOS inhibitors on the activity of CREB and c-jun in SNU-1041 cells. Cells transfected with the indicated plasmids were treated for 18 h with 1 mM L-NAME, 100 μM 1400W or 2 mM Aminoguanidine. Total cell lysates were extracted and the RLUs were measured. Luciferase activities were normalized to that of β-galactosidase

Discussion

We previously reported that NO induces COX-2 expression in cancer cells (Park *et al*., 2003). Other groups have noted that while iNOS and COX-2 are barely detectable in resting inflammatory cells, their expression levels are transiently upregulated in response to signals such as growth factors and stress (Posadas *et al*., 2000; Surh *et al*., 2001). However, we have observed that iNOS and COX-2 are constitutively overexpressed in all tested head and neck squamous cell carcinoma (HNSCC) cell lines, prompting us to question whether the regulatory mechanisms of their expression differ in inflammatory and cancer cells.

It has been well established that NF-κB, NF-IL6, PEA-3 and CREB/AP-1 are the main TFs responsible for the regulation of COX-2 expression (Howe *et al*., 2001; Tang *et al*., 2001; Tamura *et al*., 2002; Tanabe and Tohnai, 2002). In addition, a growing body of evidence indicates that NF-κB plays a central role in the general inflammatory response and may be important in the upregulation of COX-2 expression in macrophage-like cells (Chabot-Fletcher, 1996). NF-κB has been suggested to play a role in the regulation of COX-2 expression in cancer cells (Luque and Gelinas, 1997; Surh *et al*., 2001), but CRE-binding factors have been more frequently associated with COX-2 expression in these cells (Xu *et al*., 1997; Guo *et al*., 2001; Subbaramaiah *et al*., 2002). In this study, we observed that the CRE element is critical for activation of the COX-2 promoter in all cells tested. Furthermore, a mutation in the NF-κB binding site had no effect on COX-2 expression, and the NF-κB inhibitors tested in this work had no affect on expression of COX-2 (data not shown). These observations suggest that differential COX-2 expression in cancer cells may depend on epigenetic events within the regulatory region of genes or on intracellular signaling generated during carcinogenesis (Song *et al*., 2001).

We investigated whether the NO-induced overexpression of COX-2 in cancer cells was mediated by CRE

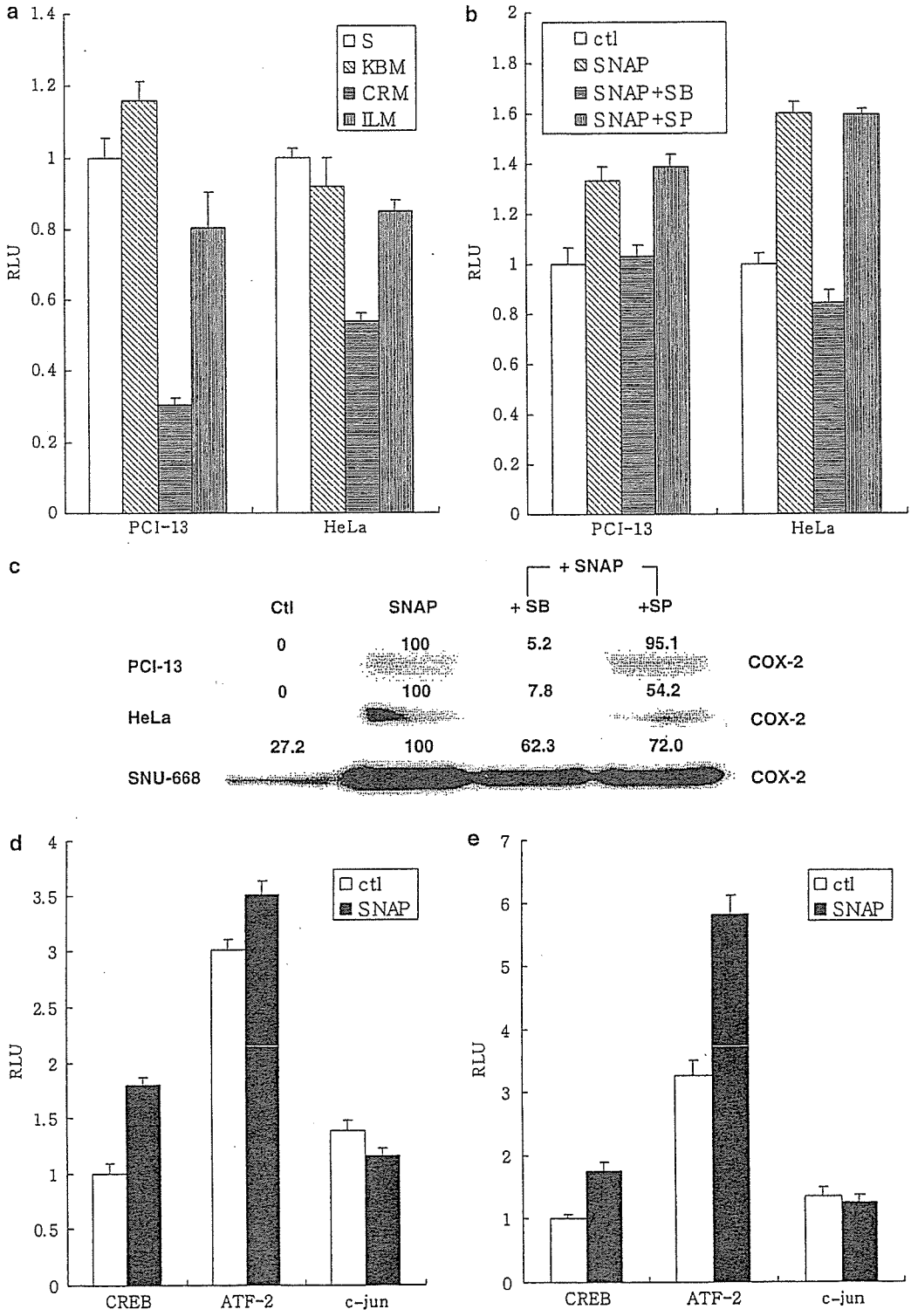

Figure 7 The effect of NO on COX-2 expression in other cancer cells. (a) The COX-2 promoter activity was measured in PCI-13 and HeLa cells transfected with a partial COX-2 promoter (−327/+59(S), KBM, CRM or ILM). (b) PCI-13 or HeLa cells transfected with the partial COX-2 promoter (−1432/+59) were treated for 18 h with 500 μM SNAP, 500 μM SNAP + 12.5 μM SB202190 or 500 μM SNAP + 10 μM SP6001125. Cell extracts were screened for COX-2 promoter activity. (c) Un-transfected PCI-13, HeLa and SNU-668 cells were treated for 18 h with 500 μM SNAP, 500 μM SNAP + 12.5 μM SB202190 or 500 μM SNAP + 10 μM SP6001125. Cell extracts (40 μg of total protein) were used for Western blotting. The variation of COX-2 expression by p38 and JNK inhibitors was analysed quantitatively by densitometry and indicated in figure. (d, e) SNAP (500 μM) was added for 18 h to (d) PCI-13 and (e) HeLa cells transfected with pFA-ATF-2, pFA2-CREB or pFA2-cJun. Cell lysates were used to determine the activity of each transcription factor

element-interacting factors. AP-1 family members bind to the CREB site in many cells (Park *et al.*, 1999). Although the CRE sequence in the COX-2 promoter (5′-TTCGTCA-3′) differs slightly from the consensus sequences for CREB (5′-TGACGTCA-3′) and AP-1 (5′-TGAGTCA-3′), studies have shown that CREB/ATF-2 and AP-1 interact with the CRE of COX-2 (Xu *et al.*, 1997; Guo *et al.*, 2001). Similarly, we observed that CREB, ATF-2 and c-jun, but not c-fos, bind to the CRE of the COX-2 promoter in the tested cells. In addition, we showed that NO activates CREB, ATF-2 and c-jun. However, the NO-induced activations of these factors appear to be regulated by different mechanisms. Phosphorylation of CREB was increased by the NO-induced activation of sGC, which subsequently activated p38 mitogen-activated protein kinase (MAPK), an upstream regulator of CREB. In contrast, c-jun was phosphorylated by the direct activation of JNK by NO, and ATF-2 activity was upregulated by both p38 and JNK (Figure 8). We were unable to identify the specific molecule linking cGMP signaling to activation of p38, but did observe that inhibition of PKC reduced p38 activation by ~30%. Previous studies reported that p38 could be activated by PKG via an unknown mechanism (Browning *et al.*, 2000). However, PKA, PKG and Ca^{2+} did not appear to be involved in NO-induced upregulation of p38, suggesting that one or more other regulator(s) may participate in the activation of p38 by cGMP in our model.

Our results indicate that NO appears to upregulate various signaling molecules, leading to activation of TFs related to CRE of COX-2 promoter and increased expression of COX-2 in cancer cell lines derived from HNSCC (SNU-1041, PCI-13), cervical cancer (HeLa), and gastric cancer (SNU-668) tissues. In addition, another group has shown that the effect of NO on PEA-3-mediated induction of COX-2 is relevant in colorectal cancer cells (Liu *et al.*, 2004). This means that NO might affect COX-2 expression in various mechanisms.

Other potential upstream regulators of COX-2 overexpression in cancer cells reportedly include epidermal growth factor (EGF) receptor activation (Coffery *et al.*, 1997), Her-2/neu activation (Vadlamudi *et al.*, 1999), p53 mutation (Han *et al.*, 2002) and ras mutation (Slice *et al.*, 2000). Interestingly, Her-2/neu activation and ras mutation both lead activation of the CRE element in the COX-2 promoter (Slice *et al.*, 2000; Subbaramaiah *et al.*, 2002).

Unlike lipopolysaccharide (LPS), EGF and PMA, which strongly induce COX-2, NO is a relatively weak inducer of COX-2 expression. While these strong inducers are capable of triggering increased COX-2 expression even in cells with low basal COX-2 expression, our data indicate that NO was only able to efficiently induce COX-2 expression in cells with moderate to strong basal COX-2 expression. We thus postulate that in cancer cells, the COX-2-inducible signaling molecules are constitutively activated such that they are sensitive to further activation by NO. In noncancerous cells, however, the NO-responsive molecules are only weakly activated and are unable to respond to NO. Thus, NO may act to accelerate existing intracellular signals rather than generating new signals.

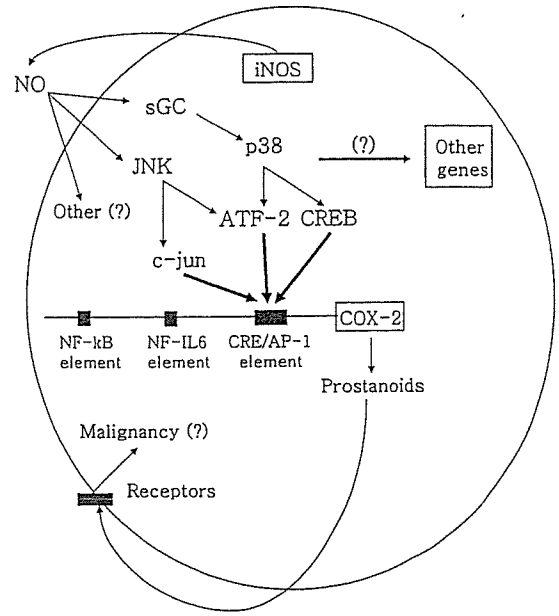

Figure 8 Possible mechanisms of NO-derived signal contributions to COX-2 expression in cancer cells. Endogenous or abnormally induced NO in the cancer microenvironment may upregulate COX-2 expression via activation of the transcription factors that associate with the CRE of the COX-2 promoter. Our data seem to suggest that NO may accelerate existing intracellular signals, rather than generating new signaling. We thus postulate that in cancer cells, NO is able to upregulate the expression of COX-2 because COX-2-inducible signaling molecules are already constitutively activated, leaving them sensitized to NO signaling. In noncancer cells, however, the NO-responsive molecules are only weakly activated, so NO is unable to induce COX-2 expression. In this way, NO may induce the expression of COX-2 and possibly other factors that promote the growth and survival of tumor cells

COX-2 is thought to play an important role in carcinogenesis, suggesting that its blockade could be beneficial in terms of cancer management. However, regulation of COX-2 expression is a complex process mediated by numerous factors, complicating efforts to clinically block COX-2 expression. Moreover, the currently available COX-2 inhibitors block both COX-1 and COX-2 in normal cells during inflammatory responses, limiting their applicability to cancer therapy. Thus, it is important to identify differences in regulation of COX-2 expression between cancerous and noncancerous cells, as these differences could allow targeting of the cancer-specific COX-2 pathway(s) for novel therapeutic strategies.

In conclusion, our data suggest that the cAMP-response element is a key regulator of COX-2 expression in cancer cells (i.e. head and neck cancer cells), and that endogenous or abnormally induced NO in the cancer microenvironment may upregulate COX-2 expression through the activation of TFs capable of binding the

CRE in the COX-2 promoter. NO appears to accelerate existing intracellular signals rather than generating new signaling, and thus may promote the growth and survival of tumor cells. These novel results suggest that additional studies on the role of NO in carcinogenesis may be warranted and that iNOS should potentially be re-evaluated as a molecular target for cancer prevention and treatment.

Materials and methods

Cell culture

HNSCC cells line SNU-1041 was obtained from the Korean Cell Line Bank (Seoul National University, Seoul, Korea) (Chung *et al.*, 2000), while HNSCC cell line PCI-13 was obtained from the Pittsburgh Cancer Institute (University of Pittsburgh, PA, USA) (Heo *et al.*, 1989). We additionally used gastric cancer cell line SNU-668 (Song *et al.*, 2001) and HeLa. All cells were cultured in DMEM or RPMI-1640 media supplemented with 10 mg/ml gentamicin and 10% fetal bovine serum (FBS). Cells were maintained at 37°C in a humidified, 5% CO_2, 95% air atmosphere and routinely subcultured using trypsin-EDTA (0.25% w/v). All cell culture reagents were obtained from Gibco BRL (Grand Island, NY, USA), unless otherwise stated.

Chemicals

SNAP (NO donor), db-cGMP, PMA, L-NAME (universal NOS inhibitor), AG (specific iNOS inhibitor), LPS and EGF were obtained from Sigma Chemical Co. (St Louis, MO, USA). ODQ (soluble guanylate cyclase (sGC) inhibitor), SB202190 (p38 MAPK inhibitor), SP600125 (JNK inhibitor), U0126 (ERK inhibitor), PD153015 (ERK inhibitor), 2′,3′-Dideoxyadenosine (2-3-DDA, PKA inhibitor), 2-[1-93-Dimethylaminopropyl]-1H-indol-3-yl)-3-(1H-indol-3-yl)-maleimide (Bisindolylmaleimide I, PKC inhibitor), Bisindolylmaleimide IX (Ro-31-8220, PKC inhibitor) and Rp-8-pCPT-cGMPs (PKG inhibitor) were obtained from Calbiochem (La Jolla, CA, USA). 1400W (specific iNOS inhibitor) was obtained from Cayman (Ann Arbor, MI, USA). Most chemicals were utilized according to the provided suggestion (IC50 and references), with the exception of SNAP and 1400W, which were applied according to our previous optimization study results (Park *et al.*, 2003).

COX-2 promoter activity assay

The COX-2 promoter constructs (−1432/+59(L), −327/+59 (S), KBM, ILM, CRM, KBM+ILM, KBM+CRM, ILM+CRM, and Triple M) were generated as previously described (Inoue *et al.*, 2000). The PGL2-Basic control vector was purchased from Promega (Madison, WI, USA), and the pSV-β galactosidase control vector was a kind gift from Dr Yung-Jue Bang (Cancer Research Institute, Seoul National University, Seoul, Korea). Cells were seeded at 10^5/well in 12-well culture plates and grown to 70–80% confluence in complete growth media containing 10% FBS. Cells were cotransfected with 0.5 μg COX-2 promoter construct and 0.5 μg pSV-β galactosidase control vector using Lipofectamine Plus according to the manufacturer's instructions (Life Technologies, Gaithersburg, MD, USA). After 4 h, medium containing 10% FBS was added and cells were incubated for an additional 20 h. Subsequently, cells were incubated in serum-free medium for 24 h and then treated for 18 h with the NO donor and/or other chemicals as indicated. Luciferase activity was measured using a TR717 Microplate Luminometer with a Bioluminescent Reporter Gene Assay kit, according to the manufacturer's instructions (Tropix, Bedford, MA, USA). The pGL2-Basic vector without insert was used as the negative control in transfection experiments. Luciferase activity was normalized according to that of β-galactosidase.

Gel shift assay

Gel shift experiments were performed using a gel shift assay system according to the manufacturer's instructions (Promega, Madison, WI, USA). Cells were harvested and nuclear extracts were prepared. We designed and synthesized double-stranded oligonucleotides containing the CRE site of the COX-2 promoter (5′-AAA CAG TCA TTT CGT CAC ATG GGC TTG-3′). Oligonucleotides containing the consensus sequences of the CREB (5′-AGA GAT TGC CTG ACG TCA GAG AGC TAG-3′), AP-1 (5′-CGC TTG ATG AGT CAG CCG GAA-3′) and NF-κB (5′-AGT TGA GGG GAC TTT CCC AGG-3′) sites were obtained from Promega (Madison, WI, USA) and used as unlabeled competitors. The complementary oligonucleotides containing the CRE of the COX-2 promoter were annealed in 20 mM Tris-Cl (pH 7.4), 50 mM NaCl, 10 mM $MgCl_2$, and 1 mM dithiothreitol. Annealed oligonucleotides were phosphorylated at the 5′-end with [γ-^{32}P]ATP and T4 polynucleotide kinase. The binding reaction was performed by incubating 5 μg of nuclear proteins with 5 × binding buffer (50 mM Tris-Cl (pH 7.5), 20% glycerol, 5 mM $MgCl_2$, 2.5 mM EDTA, 2.5 mM dithiothreitol, 250 mM NaCl and 0.25 mg/ml poly (dI-dC)) in a final volume 9 μl for 10 min at room temperature. Then, 1 μl of the labeled oligonucleotide was added to the reaction mixture and incubated for 20 min at room temperature. For the competition assay, unlabeled oligonucleotides containing the CRE of COX-2, or the CREB, AP-1 or NF-κB consensus sequences were used. The samples were incubated with anti-CREB, anti-ATF-2, anti-c-jun or anti-c-fos antibodies for 1 h, followed by addition of ^{32}P-labeled oligonucleotides containing the CRE site of COX-2. Samples were electrophoresed on a Novex 6% DNA retardation gel (Invitrogen). The gel image was transferred to an imaging plate (BAS-MP 2040S, Fuji Photo Film Co., Tokyo, Japan), and the degree of binding was calculated based on hybridization signals measured with a bio-imaging analyser (FRA2000 system, Fuji Photo Film Co., Tokyo, Japan).

TF activation assay

The fusion trans-activator plasmids (pFA-ATF-2, pFA2-CREB, and pFA2-cJun) consisting of the DNA binding domain of Gal4 (residue 1–147) and the trans-activation domains of ATF-2, CREB or c-jun were purchased from Stratagene (La Jolla, CA, USA). pFC2-dbd, which contains only the DNA binding domain of Gal4 (residue 1–147), was used as the negative control. We performed experiments according to the manufacturer's instructions.

Protein extraction and Western blot analysis

Cultured cells were rinsed with PBS, suspended in lysis buffer (0.5% NP40, 50 mM Tris-Cl, 150 mM NaCl, 1 mM dithiothreitol, 1% Triton X-100, 1% sodium deoxycholate, 0.1% SDS, 1 mM EDTA, 1 mM phenylmethylsulfonyl fluoride, 0.1 μM aprotinin, and 1 μM pepstatin A), and incubated at 4°C for 30 min. The cell lysates were then centrifuged at 13 000 r.p.m. for 20 min at 4°C, and then appropriate amount of supernatant (determined by protein assay) was mixed with 4 × sample loading buffer and denatured for 10 min at 70°C. The

denatured protein samples were fractionated on 4–12% NuPAGE gels (Invitrogen, Carlsbad, CA, USA), transferred onto nitrocellulose membranes (Schleicher & Schuell, Dachen, Germany) and incubated with Tris-buffered saline containing 0.1% Tween-20 and 5% nonfat dry milk. The membranes were then incubated with anti-COX-2, anti-p38, anti-phospho-p38, anti-JNK, anti-phospho-JNK, anti-c-fos (all from Santa Cruz Biotechnology, Santa Cruz, CA, USA), monoclonal anti-α-tubulin (Sigma Chemical Co., St Louis, MO, USA), anti-CREB, anti-phospho-CREB, anti-ATF-2, anti-phospho-ATF-2, anti-c-jun or anti-phospho-c-jun (all from Cell Signaling Technology, Beverly, MA, USA) for 2 h at room temperature or overnight at 4°C. Membranes were then washed (4 × 15 min) with 1 × TBS-T and incubated with horseradish peroxidase-conjugated secondary antibody (Pierce, Rockford, IL, USA) for 1 h. Immunoreactive proteins were visualized by development with the lumi-light Western blotting substrate (Roche Diagnostics GmbH, Mannheim, Germany) and exposure to X-ray film.

Statistical analysis

The data are presented as the mean ± standard deviation (s.d.) of triplicates, or as a representative of three separate experiments. Levels of significance were determined between treated and untreated groups by two-sided Student's *t*-test.

Abbreviations

NO, nitric oxide; iNOS, inducible nitric oxide synthase; COX-2, cyclooxygenase-2; CRE, cAMP-response element; sGC, soluble guanylate cyclase; PGE_2, prostaglandin E_2; HNSCC, head and neck squamous cell carcinoma; MAPK, mitogen-activated protein kinase; ERK, extracellular signal-regulated kinase; JNK, c-Jun NH_2-terminal kinase; CREB, cAMP response element-binding protein; ATF-2, activating transcription factor-2; AP-1, activator protein-1; PKA, cAMP-dependent protein kinase; PKC, protein kinase-C; PKG, protein kinase G.

Acknowledgements

We thank Dr Lee Jung Weon (Cancer Research Institute, Seoul National University, Seoul, Korea) for helpful discussion. This work was supported in part by a Korea Research Foundation Grant (KRF-2002-041-E00134) and by BK21 project for Medicine, Dentistry and Pharmacy, Korea.

References

Bogdan C. (2001). *Trends Cell Biol.*, **11**, 66–75.
Browning DD, Mcshane MP, Marty C and Ye RD. (2000). *J. Biol. Chem.*, **275**, 2811–2816.
Chabot-Fletcher M. (1996). *Pharmacol. Rev. Commun.*, **8**, 317–324.
Chan G, Boyle JO, Yang EK, Zhang F, Sachs PG, Shah JP, Edelstein D, Soslow RA, Koki AT, Woerner BM, Masferrer JL and Dannenberg AJ. (1999). *Cancer Res.*, **59**, 991–994.
Chung PS, Rhee CK, Kim KH, Paek W, Chung J, Paiva MB, Eshraghi AA, Castro DJ and Saxton RE. (2000). *Laryngoscope*, **110**, 1312–1316.
Coffery RJ, Hawkey CJ, Damstrup L, Graves-Deal R, Daniel VC, Dempsey PJ, Chinery R, Kirkland SC, DuBois RN, Jetton TL and Morrow JD. (1997). *Proc. Natl. Acad. Sci. USA*, **94**, 657–662.
Gallo O, Masini E, Morbidelli L, Franchi A, Fini-Storchi I, Vergari WA and Ziche M. (1998). *J. Natl. Cancer Inst.*, **90**, 587–596.
Guo YS, Hellmich MR, Wen XD and Townsend Jr CM. (2001). *J. Biol. Chem.*, **276**, 22941–22947.
Habib A, Bernard C, Lebret M, Creminon C, Esposito B, Tedgui A and Maclouf J. (1997). *J. Immunol.*, **158**, 3845–3851.
Han JA, Kim JI, Ongusaha PP, Hwang DH, Ballou LR, Mahale A, Aaronson SA and Lee SW. (2002). *EMBO J.*, **21**, 5635–5644.
Heo DS, Snyderman C, Gollin SM, Pan S, Walker E, Deka R, Barnes EL, Johnson JT, Herberman RB and Whiteside TL. (1989). *Cancer Res.*, **49**, 5167–5175.
Howe LR, Crawford HC, Subbaramaiah K, Hassell JA, Dannenberg AJ and Brown AM. (2001). *J. Biol. Chem.*, **276**, 20108–20115.
Inoue H, Tanabe T and Umesono K. (2000). *J. Biol. Chem.*, **275**, 28028–28032.
Lee DW, Sung MW, Park SW, Seong WJ, Roh JL, Park BJ, Heo DS and Kim KH. (2002). *Anticancer Res.*, **22**, 2089–2096.
Liaudet L, Soriano FG and Szabo C. (2000). *Crit. Care Med.*, **28** (Suppl), N37–N52.
Liu Y, Borchert GL and Phang JM. (2004). *J. Biol. Chem.*, **279**, 18694–18700.
Luque I and Gelinas C. (1997). *Semin. Cancer Biol.*, **8**, 103–111.
Nose F, Ichikawa T, Fujiwara M and Okayasu I. (2002). *Am. J. Clin. Pathol.*, **117**, 546–551.
Pai R, Soreghan B, Szabo IL, Pavelka M, Baatar D and Tarnawski AS. (2002). *Nat. Med.*, **8**, 289–293.
Park SW, Lee SG, Song SH, Heo DS, Park BJ, Lee DW, Kim KH and Sung MW. (2003). *Int. J. Cancer*, **107**, 729–738.
Park YK, Nesterova M, Agrawal S and Cho-Chung YS. (1999). *J. Biol. Chem.*, **274**, 1573–1580.
Posadas I, Terencio MC, Guillen I, Ferrandiz ML, Coloma J, Paya M and Alcaraz MJ. (2000). *Naunyn-Schied. Arch. Pharmacol.*, **361**, 98–106.
Salvemini D, Misko TP, Masferrer JL, Seibert K, Currie MG and Needleman P. (1993). *Proc. Natl. Acad. Sci. USA*, **90**, 7240–7244.
Sheng H, Shao J, Washington MK and DuBois RN. (2001). *J. Biol. Chem.*, **276**, 18075–18081.
Slice LW, Bui L, Mak C and Walsh JH. (2000). *Biochem. Biophys. Res. Commun.*, **276**, 406–410.
Son HJ, Kim YH, Park DI, Kim JJ, Rhee PL, Paik SW, Choi KW, Song SY and Rhee JC. (2001). *J. Clin. Gastroenterol.*, **33**, 383–388.
Song SH, Jong HS, Choi HH, Inoue H, Tanabe T, Kim NK and Bang YJ. (2001). *Cancer Res.*, **61**, 4628–4635.
Stadler J, Harbrecht BG, DiSilvio M, Curran RD, Jordan ML, Simmons RL and Billiar TR. (1993). *J. Leukocyte Biol.*, **53**, 165–172.
Subbaramaiah K, Norton L, Gerald W and Dannenberg AJ. (2002). *J. Biol. Chem.*, **277**, 18649–18657.
Sun Y, Tang XM, Elizabeth HM, Kuo T and Sinicrope FA. (2002). *Cancer Res.*, **62**, 6323–6328.
Surh YJ, Chun KS, Cha HH, Han SS, Keum YS, Park KK and Lee SS. (2001). *Mutat. Res.*, **480–481**, 243–268.
Tamura M, Sbastian S, Yang S, Gutates B, Ferrer K, Sasano H, Okamura K and Bulun SE. (2002). *J. Biol. Chem.*, **277**, 26208–26216.

Tanabe T and Tohnai N. (2002). *Prostaglandins Other Lipid Mediators*, **68–69**, 95–114.
Tang Q, Chen W, Gonzales MS, Finch J, Inoue H and Bowden GT. (2001). *Oncogene*, **20**, 5164–5172.
Tsai AL, Wei C and Kulmacz RJ. (1994). *Arch. Biochem. Biophys.*, **313**, 367–372.
Vadlamudi R, Mandal M, Adam L, Steinbach G, Mendelsohn J and Kumar R. (1999). *Oncogene*, **18**, 305–314.
Wink DA, Vodovotz Y, Laval J, Laval F, Dewhirst MW and Mitchell JB. (1998). *Carcinogenesis*, **19**, 711–721.
Xu XM, Tang JL, Chen X, Wang LH and Wu KK. (1997). *J. Biol. Chem.*, **272**, 6943–6950.

Intense quasi-monochromatic flash x-ray generator utilizing molybdenum-target diode

Michiaki Sagae*[a], Eiichi Sato[a], Haruo Obara[b], Etsuro Tanaka[c], Hidezo Mori[d], Toshiaki Kawai[e], Shigehiro Sato[f], Hidenori Ojima[g], Kazuyoshi Takayama[g] and Hideaki Ido[h]

[a] Department of Physics, Iwate Medical University, 3-16-1 Honchodori, Morioka 020-0015, Japan
[b] Department of Radiological Technology, College of Medical Science, Tohoku University, 1-1 Seiryocho, Sendai 980-0872, Japan
[c] Department of Nutritional Science, Faculty of Applied Bio-science, Tokyo University of Agriculture, 1-1-1 Sakuragaoka, Setagaya-ku 156-8502, Japan
[d] Department of Cardiac Physiology, National Cardiovascular Center Research Institute, 5-7-1 Fujishirodai, Suita, Osaka 565-8565 Japan
[e] Electron Tube Division #2, Hamamatsu Photonics K. K., 314-5 Shimokanzo, Toyooka Village, Iwata-gun 438-0193, Japan
[f] Department of Microbiology, School of Medicine, Iwate Medical University, 19-1 Uchimaru, Morioka 020-8505, Japan
[g] Shock Wave Research Center, Institute of Fluid Science, Tohoku University, 2-1-1 Katahira, Sendai 980-8577, Japan
[h] Department of Applied Physics and Informatics, Faculty of Engineering, Tohoku Gakuin University, 1-13-1 Chuo, Tagajo 985-8537, Japan

ABSTRACT

In the flash x-ray generator, a 150 nF condenser is charged up to 80 kV by a power supply, and flash x rays are produced by the discharging. The x-ray tube is a demountable diode, and the turbomolecular pump evacuates air from the tube with a pressure of approximately 1 mPa. Since the electric circuit of the high-voltage pulse generator employs a cable transmission line, the high-voltage pulse generator produces twice the potential of the condenser charging voltage. At a charging voltage of 80 kV, the estimated maximum tube voltage and current were approximately 160 kV and 40 kA, respectively. When the charging voltage was increased, the K-series characteristic x-ray intensities of molybdenum increased. The K lines were clean and intense, and hardly any bremsstrahlung rays were detected at all. The x-ray pulse widths were approximately 100 ns, and the time-integrated x-ray intensity had a value of approximately 15 μC/kg at 1.0 m from the x-ray source with a charging voltage of 80 kV.

Keywords: flash x-ray, energy-selective radiography, characteristic x rays, quasi-monochromatic x rays, bremsstrahlung x-ray distribution

1. INTRODUCTION

In recent years, there have been several investigations dealing with the production of monochromatic x rays in radiology and cardiology. Particularly, monochromatic parallel beams using synchrotrons have been employed to perform enhanced K-edge angiography[1,2] and x-ray phase imaging.[3,4] In angiography, parallel beams with photon energies of approximately 35 keV have been employed, since these beams are absorbed effectively by an iodine-based contrast medium. Subsequently, in cases where phase imaging is employed, the spatial resolution can be improved, and the number of tissues which can be observed using x rays increases.
In order to perform biomedical radiography, we have developed several different soft flash x-ray generators[5-10] corresponding to specific radiographic objectives. Subsequently, electron impact flash x-ray sources can produce quasi-monochromatic x rays, because bremsstrahlung rays are not emitted in the opposite direction to that of electron

26th International Congress on High-Speed Photography and Photonics, edited by D. L. Paisley, S. Kleinfelder, D. R. Snyder, B. J. Thompson, Proc. of SPIE Vol. 5580 (SPIE, Bellingham, WA, 2005) · 0277-786X/05/$15 · doi: 10.1117/12.581246

acceleration.[11] Therefore, the sources will be conventional x-ray tubes for producing cone-beam K-series characteristic x rays, and monochromatic Kα rays are obtained using a K-edge filter.
We have developed several different plasma flash x-ray generators[12-16] corresponding to specific radiographic objectives, and a major goal in our research is the development of an intense and sharp monochromatic x-ray generator that can impact applications with biomedical radiography. By forming weakly ionized linear plasma, because we have succeeded in producing fairly intense and clean K-series characteristic x rays. Without forming the linear plasma, characteristic x rays can be produced by considering the angle dependence of bremsstrahlung x rays. On the other hand, the electrostatic energy in the main discharge condenser should be increased as much as possible to increase the characteristic x-ray intensity.
In this paper, we describe an intense single flash x-ray generator utilizing a rod-target radiation tube, used to perform a preliminary experiment for generating intense and clean molybdenum K-series characteristic x rays.

2. GENERATOR

2.1 High-voltage circuit

Figure 1 shows a block diagram of a high-intensity plasma flash x-ray generator. The generator consists of the following essential components: a high-voltage power supply, a high-voltage condenser with a capacity of approximately 150 nF, an air gap switch, a turbomolecular pump, a thyratron pulse generator as a trigger device, and a flash x-ray tube. In this generator, a coaxial cable transmission line is employed in order to increase maximum tube voltage using high-voltage reflection. The high-voltage main condenser is charged up to 80 kV by the power supply, and electric charges in the condenser are discharged to the tube through the four cables after closing the gap switch with the trigger device (Fig. 2).

2.2 X-ray tube

The x-ray tube is a demountable cold-cathode diode that is connected to the turbomolecular pump with a pressure of approximately 1 mPa (Fig. 3). This tube consists of the following major parts: a ring-shaped graphite cathode with an inside diameter of 4.5 mm, a stainless-steel vacuum chamber, a nylon insulator, a polyethylene terephthalate (Mylar) x-ray window 0.25 mm in thickness, and a rod-shaped molybdenum target 3.0 mm in diameter. The distance between the target and cathode electrodes can be regulated from the outside of the tube, and is set to 1.5 mm. As electron beams from the cathode electrode are roughly converged to the target by the electric field in the tube, evaporation leads to the formation of weakly ionized plasma, consisting of molybdenum ions and electrons, around the target. Because bremsstrahlung rays are not emitted in the opposite direction to that of electron acceleration (Fig. 4), molybdenum K-series characteristic x rays can be produced without using a filter.

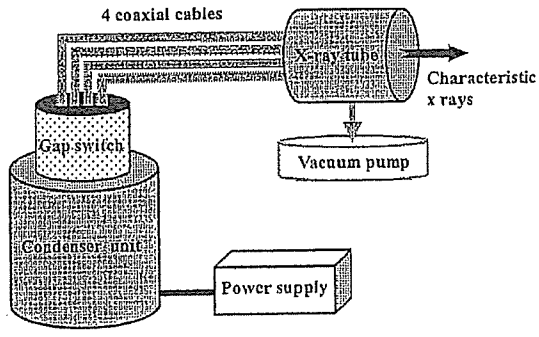

Figure 1: Block diagram of intense quasi-monochromatic flash x-ray generator.

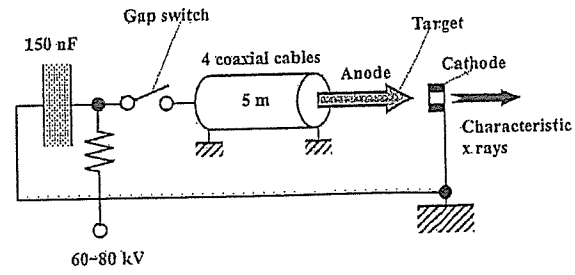

Figure 2: Circuit diagram of flash x-ray generator.

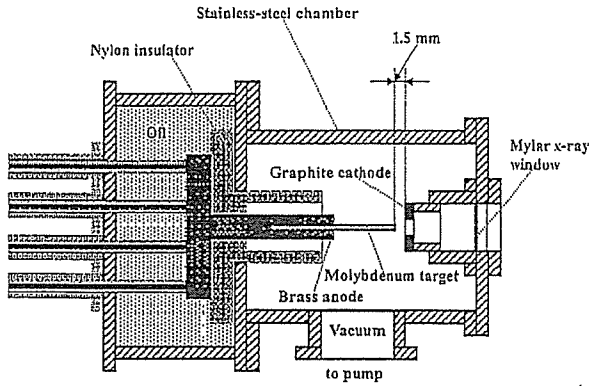

Figure 3: Schematic drawing of flash x-ray tube.

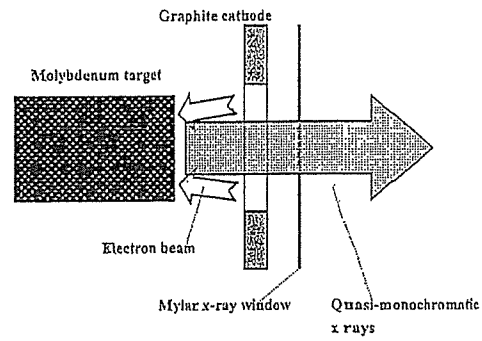

Figure 4: Irradiation of characteristic x rays.

3. CHARACTERISTICS

3.1 Tube voltage and current

In this generator, it was difficult to measure the tube voltage and current since the tube voltages were high, and there was no space to set a current transformer for measuring the tube current. Currently, the voltage and current roughly displayed damped oscillations. When the charging voltage was increased, both the maximum tube voltage and current increased. At a charging voltage of 80 kV, the estimated maximum values of the tube voltage and current were approximately 160 kV (2 times the charging voltage) and 40 kA, respectively.

3.2 X-ray output

X-ray output pulse was detected using a combination of a plastic scintillator and a photomultiplier (Fig. 5). The x-ray pulse height increased with corresponding increases in the charging voltage. The x-ray pulse widths were approximately 100 ns, and the time-integrated x-ray intensity measured by a thermoluminescence dosimeter (Kyokko TLD Reader 1500 having MSO-S elements without energy compensation) had a value of approximately 15 μC/kg at 1.0 m from the x-ray source with a charging voltage of 80 kV.

3.3 X-ray source

In order to observe the characteristic x-ray source, we employed a 100-μm-diameter pinhole camera and an x-ray film (Polaroid XR-7) (Fig. 6). When the charging voltage was increased, the plasma x-ray source grew, and both spot dimension and intensity increased. Because the x-ray intensity is the highest at the center of the spot, both the dimension and intensity decreased according to both increases in the thickness of a filter for absorbing x rays and decreases in the pinhole diameter.

3.4 X-ray spectra

X-ray spectra were measured by a transmission-type spectrometer with a lithium fluoride curved crystal 0.5 mm in thickness. The spectra were taken by a computed radiography (CR) system (Konica Regius 150)[17] with a wide dynamic range, and relative x-ray intensity was calculated from Dicom digital data. Figure 7 shows measured spectra from the molybdenum target. We observed clean K-series lines, while bremsstrahlung rays were hardly detected at all. The characteristic x-ray intensity substantially increased with increases in the charging voltage.

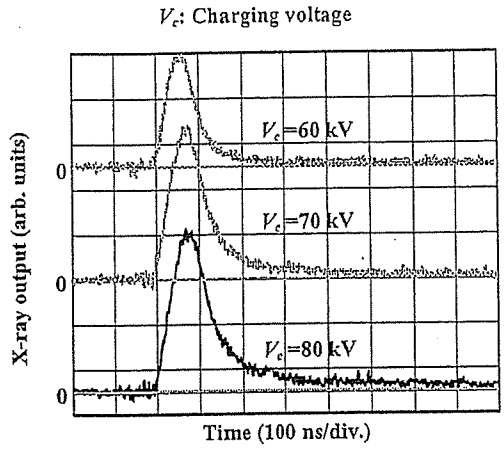

Figure 5: X-ray outputs at indicated conditions.

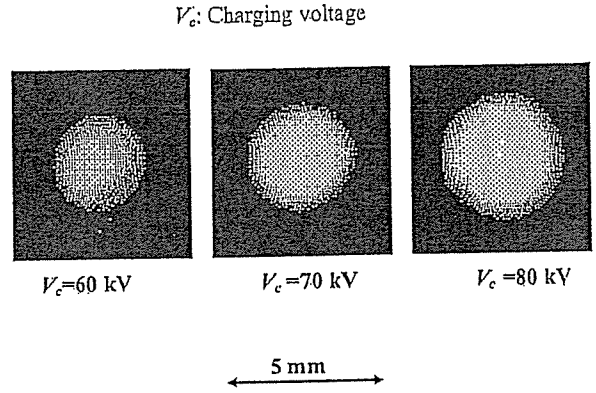

Figure 6: Images of characteristic x-ray source.

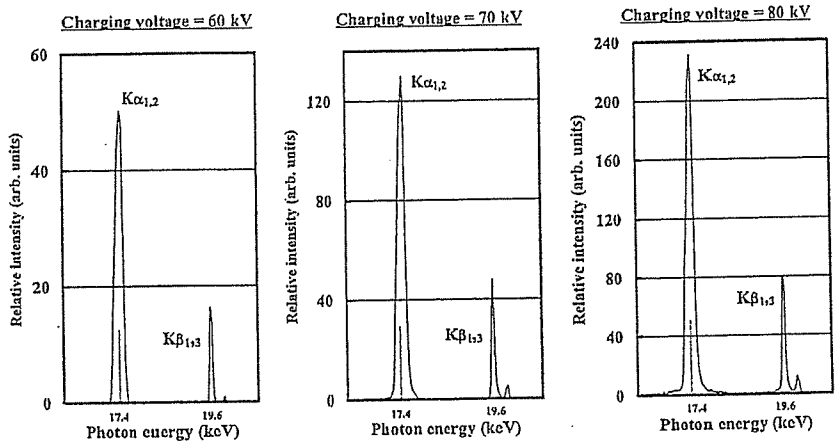

Figure 7: X-ray spectra from molybdenum target.

4. RADIOGRAPHY

The quasi-monochromatic flash radiography was performed by the CR system at 1.2 m from the x-ray source. Firstly, rough measurements of spatial resolution were made using wires. Figure 8 shows radiograms of tungsten wires coiled around a pipe made of polymethyl methacrylate with a charging voltage (V_c) of 70 kV. Although the image contrast increased with increases in the wire diameter, a 50-μm-diameter wire could be observed.

Figure 9 shows a radiogram of a vertebra with a V_c of 70 kV, and fine structures in the vertebra were observed. Figures 10 and 11 shows an angiogram of a rabbit heart (V_c=70 kV) and thigh (V_c=80 kV), respectively. In angiography, iodine-based microspheres of 15 μm in diameter were used, and fine blood vessels of about 100 μm were visible. Next, the image of aluminum grains falling into a polypropylene beaker from a glass test tube with a V_c of 80 kV is shown in Fig. 12. Because the x-ray duration was approximately 100 ns, the stop-motion image of grains could be obtained.

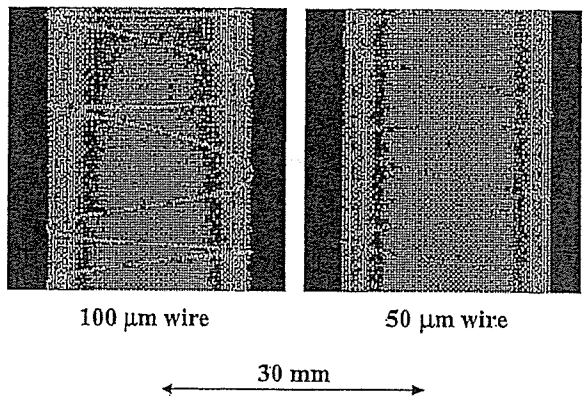

Figure 8: Radiograms of tungsten wires coiled around pipe made of polymethyl methacrylate.

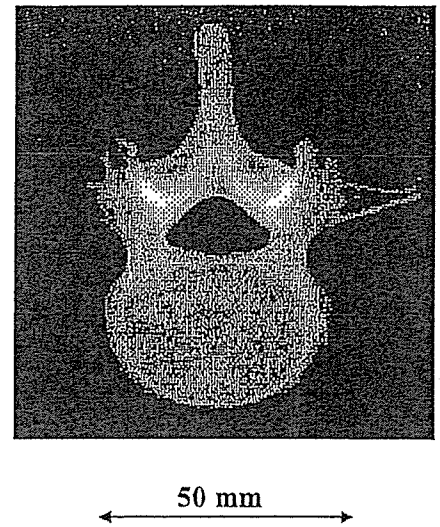

Figure 9: Radiogram of vertebra.

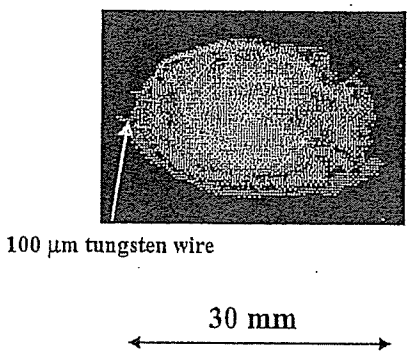

Figure 10: Angiograms of rabbit heart.

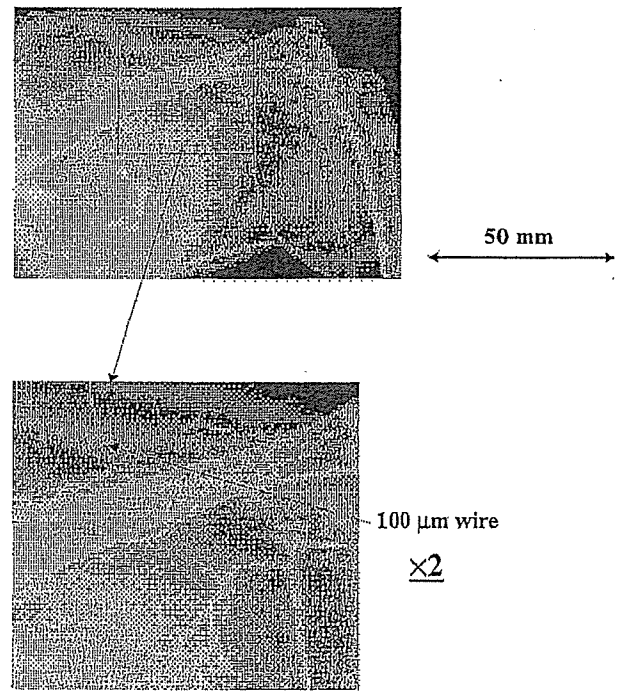

Figure 11: Angiograms of rabbit thigh.

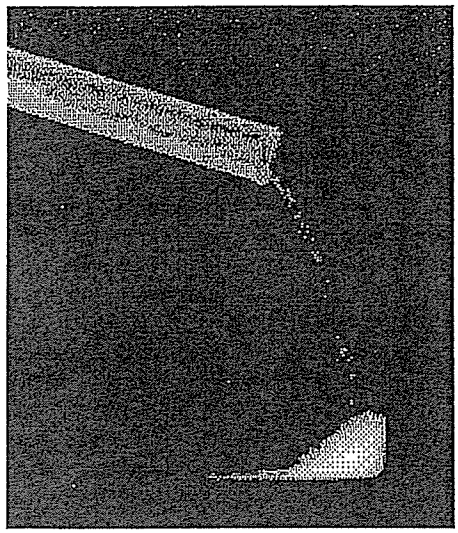

Figure 12:. Radiogram of aluminum grains falling into polypropylene beaker from glass test tube.

5. DISCUSSION

Concerning the spectrum measurement, we obtained fairly clean molybdenum Kα (17.4 keV) and Kβ (19.6 keV) lines. Therefore, we are very interested in the measurement the characteristic rays from nickel, copper, silver, cerium, and tungsten targets; the target element should be selected corresponding to the radiographic objectives. In a medical application, K-series characteristic x rays of cerium are absorbed effectively by an iodine-based contrast medium with a K-edge of 33.2 keV, and enhanced K-edge angiography can be performed.

In this research, the generator produced instantaneous number of K photons was approximately 2×10^8 photons/cm^2 per pulse at 1.0 m from the source. Subsequently, the intensity can be increased by increasing the electrostatic energy in condenser, and monochromatic Kα lines are left using a zirconium filter with a K-edge of 17.9 keV.

Using this flash x-ray generator, the photon energy of characteristic x rays can be selected, and we plan to design a high-speed photon-counting radiography system in order to decrease noise from radiograms. As compared with a steady-state x-ray generator, demonstrations of various monochromatic radiography will be accomplished easily, since the target element can be changed easily.

ACKNOWLEDGMENT

This work was supported by Grants-in-Aid for Scientific Research (13470154, 13877114, 16591181, and 16591222) and Advanced Medical Scientific Research from MECSST, Health and Labor Sciences Research Grants(RAMT-nano-001, RHGTEFB-genome-005 and RHGTEFB-saisei-003), Grants from Keiryo Research Foundation, The Promotion and Mutual Aid Corporation for Private Schools of Japan, Japan Science and Technology Agency (JST), and New Energy and Industrial Technology Development Organization (NEDO, Industrial Technology Research Grant Program in '03).

REFERENCES

1. H. Mori, K. Hyodo, E. Tanaka, M. U. Mohammed, A. Yamakawa, Y. Shinozaki, H. Nakazawa, Y. Tanaka, T. Sekka, Y. Iwata, S. Honda, K. Umetani, H. Ueki, T. Yokoyama, K. Tanioka, M. Kubota, H. Hosaka, N. Ishizawa and M. Ando, "Small-vessel radiography in situ with monochromatic synchrotoron radiation," *Radiology*, **201**, 173-177, 1996.

2. K. Hyodo, M. Ando, Y. Oku, S. Yamamoto, T. Takeda, Y. Itai, S. Ohtsuka, Y. Sugishita and J. Tada, "Development of

a two-dimensional imaging system for clinical applications of intravenous coronary angiography using intense synchrotron radiation produced by a multipole wiggler," *J. Synchrotron Rad.*, **5**, 1123-1126, 1998.
3. A. Momose, T. Takeda, Y. Itai and K. Hirano, "Phase-contrast x-ray computed tomography for observing biological soft tissues," *Nature Medicine*, **2**, 473-475, 1996.
4. M. Ando, A. Maksimenko, H. Sugiyama, W. Pattanasiriwisawa, K. Hyodo and C. Uyama, "A simple x-ray dark- and bright- field imaging using achromatic Laue optics, *Jpn. J. Appl. Phys.*, **41**, L1016-L1018, 2002.
5. E. Sato, H. Isobe and F. Hoshino, "High intensity flash x-ray apparatus for biomedical radiography," *Rev. Sci. Instrum.*, **57**, 1399-1408, 1986.
6. E. Sato, S. Kimura, S. Kawasaki, H. Isobe, K. Takahashi, Y. Tamakawa and T. Yanagisawa, "Repetitive flash x-ray generator utilizing a simple diode with a new type of energy-selective function," *Rev. Sci. Instrum.*, **61**, 2343-2348, 1990.
7. E. Sato, M. Sagae, K. Takahashi, T. Oizumi, H. Ojima, K. Takayama, Y. Tamakawa, T. Yanagisawa, A. Fujiwara and K. Mitoya, "High-speed soft x-ray generators in biomedicine," *SPIE*, **2513**, pp. 649-667, 1994.
8. A. Shikoda, E. Sato, M. Sagae, T. Oizumi, Y. Tamakawa and T. Yanagisawa, "Repetitive flash x-ray generator having a high-durability diode driven by a two-cable-type line pulser," *Rev. Sci. Instrum.*, **65**, 850-856, 1994.
9. E. Sato, K. Takahashi, M. Sagae, S. Kimura, T. Oizumi, Y. Hayasi, Y. Tamakawa and T. Yanagisawa, "Sub-kilohertz flash x-ray generator utilizing a glass-enclosed cold-cathode triode," *Med. & Biol. Eng. & Comput.*, **32**, 289-294, 1994.
10. K. Takahashi, E. Sato, M. Sagae, T. Oizumi, Y. Tamakawa and T. Yanagisawa, "Fundamental study on a long-duration flash x-ray generator with a surface-discharge triode," *Jpn. J. Appl. Phys.*, **33**, 4146-4151, 1994.
11. E. Sato, M. Sagae, E. Tanaka, Y. Hayasi, R. Germer, H. Mori, T. Kawai, T. Ichimaru, S. Sato, K. Takayama and H. Ido: Quasi-monochromatic flash x-ray generator utilizing a disk-cathode molybdenum tube, *Jpn. J. Appl. Phys.*, **43**, 7324-7328, 2004.
12. E. Sato, Y. Hayasi, R. Germer, E. Tanaka, H. Mori, T. Kawai, H. Obara, T. Ichimaru, K. Takayama and H. Ido, "Intense characteristic x-ray irradiation from weakly ionized linear plasma and applications," *Jpn. J. Med. Imag. Inform. Sci.*, **20**, 148-155, 2003.
13. E. Sato, Y. Hayasi, R. Germer, E. Tanaka, H. Mori, T. Kawai, H. Obara, T. Ichimaru, K. Takayama and H. Ido, "Irradiation of intense characteristic x-rays from weakly ionized linear molybdenum plasma," *Jpn. J. Med. Phys.*, **23**, 123-131, 2003.
14. E. Sato, Y. Hayasi, R. Germer, E. Tanaka, H. Mori, T. Kawai, T. Ichimaru, K. Takayama and H. Ido, "Quasi-monochromatic flash x-ray generator utilizing weakly ionized linear copper plasma," *Rev. Sci. Instrum.*, **74**, 5236-5240, 2003.
15. E. Sato, R. Germer, Y. Hayasi, Y. Koorikawa, K. Murakami, E. Tanaka, H. Mori, T. Kawai, T. Ichimaru, F. Obata, K. Takahashi, S. Sato, K. Takayama and H. Ido: Weakly ionized plasma flash x-ray generator and its distinctive characteristics. *SPIE*, **5196**, 383-392, 2003.
16. E. Sato, Y. Hayasi, R. Germer, E. Tanaka, H. Mori, T. Kawai, T. Ichimaru, S. Sato, K. Takayama and H. Ido, "Sharp characteristic x-ray irradiation from weakly ionized linear plasma," *J. Electron Spectrosc. Related Phenom.*, **137-140**, 713-720, 2004.
17. E. Sato, K. Sato and Y. Tamakawa, "Film-less computed radiography system for high-speed imaging," *Ann. Rep. Iwate Med. Univ. Sch. Lib. Arts and Sci.*, **35**, 13-23, 2000.
*msagae@iwate-med.ac.jp; phone, phone +81-19-651-5111; fax +81-19-654-9282

Japanese Journal of Applied Physics
Vol. 44, No. 1A, 2005, pp. 446–449

Quasi-Monochromatic X-Ray Generator Utilizing Graphite Cathode Diode with Transmission-Type Molybdenum Target

Michiaki SAGAE, Eiichi SATO, Etsuro TANAKA[1], Yasuomi HAYASI, Hidezo MORI[2], Toshiaki KAWAI[3], Toshio ICHIMARU[4], Shigehiro SATO[5], Kazuyoshi TAKAYAMA[6] and Hideaki IDO[7]

Department of Physics, Iwate Medical University, 3-16-1 Honchodori, Morioka 020-0015, Japan
[1]*Department of Nutritional Science, Faculty of Applied Bio-science, Tokyo University of Agriculture, 1-1-1 Sakuragaoka, Setagaya-ku 156-8502, Japan*
[2]*Department of Cardiac Physiology, National Cardiovascular Center Research Institute, 5-7-1 Fujishiro-dai, Suita, Osaka 565-8565, Japan*
[3]*Electron Tube Division #2, Hamamatsu Photonics K.K., 314-5 Shimokanzo, Toyooka Village, Iwata-gun 438-0193, Japan*
[4]*Department of Radiological Technology, School of Health Sciences, Hirosaki University, 66-1 Honcho, Hirosaki 036-8564, Japan*
[5]*Department of Microbiology, School of Medicine, Iwate Medical University, 19-1 Uchimaru, Morioka 020-8505, Japan*
[6]*Shock Wave Research Center, Institute of Fluid Science, Tohoku University, 2-1-1 Katahira, Aoba-ku, Sendai 980-8577, Japan*
[7]*Department of Applied Physics and Informatics, Faculty of Engineering, Tohoku Gakuin University, 1-13-1 Chuo, Tagajo 985-8537, Japan*

(Received June 19, 2004; accepted October 15, 2004; published January 11, 2005)

An X-ray generator consists of a negative high-voltage power supply and a field-emission-type cold-cathode X-ray tube. The tube is a glass-enclosed diode utilizing a transmission-type molybdenum target with a thickness of 20 μm, a needle graphite (carbon) cathode, a glass tube body, and a 0.5-mm-thick beryllium window. The tube current decreases gradually with time. After aging for 30 minutes, the tube current was approximately 0.2 mA with a tube voltage of 25 kV, and the focal-spot dimensions were 2.2 × 1.6 mm. Characteristic X-rays of molybdenum K-series were obtained after penetrating the molybdenum target and the beryllium window, and the K-absorption edge was observed clearly. The generator produced number of K photons was approximately 4×10^6 photons/cm^2·s at 1.0 m from the source. The average photon energies of Kα and Kβ lines were 17.4 and 19.6 keV, respectively, and quasi-monochromatic radiography was performed using a computed radiography system. [DOI: 10.1143/JJAP.44.446]

KEYWORDS: quasi-monochromatic X-rays, characteristic molybdenum X-rays, field emission, transmission target, quasi-monochromatic radiography

1. Introduction

Conventional medical X-ray tubes enable the observation of parts of the inside of the human body that cannot be seen by other ways. The X-ray images obtained with these tubes are exposed by both the bremsstrahlung and characteristic X-rays, unless monochromatic radiography is specifically performed. Monochromatic parallel X-ray beams are produced by synchrotrons using single crystals, and these beams have been employed to perform enhanced K-edge angiography[1–3] and X-ray phase imaging.[4,5] Subsequently, monochromatic X-ray computed tomography at two different energies has provided information on the electron density of human tissue.[6] In addition, a compact pulsed tunable monochromatic X-ray source has been designed, developed, and tested.[7] From the source, conical X-ray beams from 10 to 50 keV with pulse widths of 8 ps have been produced, and these beams are useful for biomedical imaging and protein crystallography.

Currently, flash X-ray generators[8–12] utilize cold-cathode radiation tubes and produce extremely high-dose-rate X-ray pulses with durations of less than 1 μs. In order to produce monochromatic X-rays, plasma flash X-ray generators are useful, since intense and sharp characteristic X-rays have been produced from weakly ionized linear plasmas of nickel,[13] copper[14] and molybdenum,[15] while bremsstrahlung rays are rarely detected.

In order to produce steady-state X-rays using a cold-cathode tube, the combination of the target and cathode electrodes is a very important factor. In view of the cathode, a carbon nanotube[16] is a useful field emitter and can be used as a cold cathode in an X-ray tube. Without using nanotubes, electrons can be emitted comparatively easily when lines of electric force are concentrated on a needle tip. Characteristic K-series X-rays have been obtained using a filter made of the same element as the target.

In the present research, we developed a cold-cathode X-ray tube with a needle-shaped graphite cathode, and applied it to produce characteristic molybdenum K-series X-rays by uisng a transmission target.

2. Generator

Figure 1 shows the block diagram of the X-ray generator, which consists of a negative high-voltage power supply (Model 500, −100 kV-3 mA, Pulse Electric Eng. Inc.) with dimensions of 450 × 430 × 150 mm and an X-ray tube. In the X-ray tube, the negative high voltage is applied to the cathode electrode, and the anode (target) is connected to the ground potential.

The X-ray tube is a cold-cathode diode type, as illustrated in Fig. 2. In order to perform soft radiography, including mammography, we developed a quasi-monochromatic X-ray tube with a molybdenum target. This tube consists of the following major devices: a needle-shaped graphite cathode with a tip angle of 54° and a diameter of 3.0 mm, a

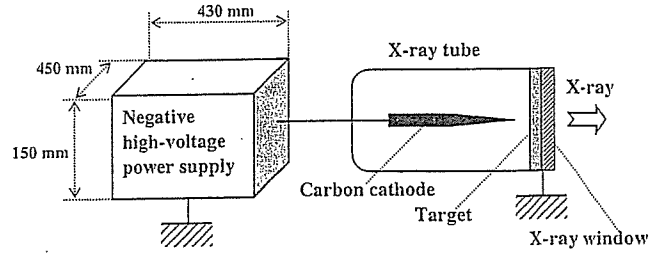

Fig. 1. Block diagram of quasi-monochromatic X-ray generator with cold-cathode diode.

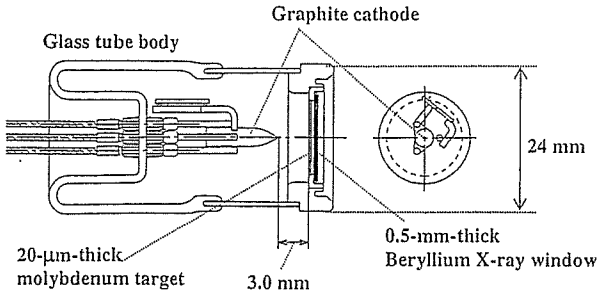

Fig. 2. Structure of X-ray tube.

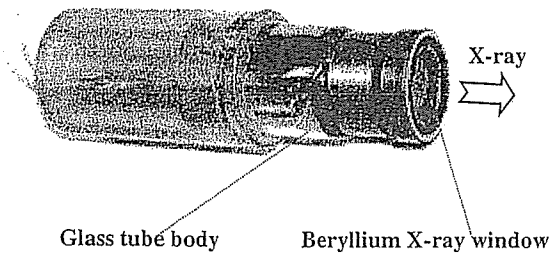

Fig. 3. Cold-cathode X-ray tube with transmission-type molybdenum target.

molybdenum disk target 20 μm thick, and a glass tube body. The target-cathode distance is 3.0 mm, and the transmission X-rays are obtained after the beam passes through the target and a 0.5-mm-thick beryllium X-ray window (Fig. 3). In this case, since the target plays the role of a K-edge filter for effectively absorbing bremsstrahlung X-rays with energies higher than the K-absorption edge, characteristic K-series X-rays are produced. The pressure in the glass-enclosed tube is primarily determined by the pressure when evacuation is stopped, and is approximately 1×10^{-4} Pa. The tube voltage is always constant and is regulated by the constant voltage power supply. Subsequently, the tube current is primarily determined by the tube voltage and the target-cathode distance, and increases with decreasing distance and increasing voltage.

In this experiment, the tube voltage applied was from 20 to 30 kV, and the exposure time was controlled in order to obtain optimum X-ray intensity for radiography.

3. Characteristics

3.1 X-ray intensity

In the field emission X-ray tube, it was very difficult to measure the X-ray intensity correctly, since the intensity gradually decreased during exposure, and small-scale vacuum breakdown may often occur. The X-ray intensity was measured using a Solidose 308 M ionization chamber for mammography at 1.0 m from the X-ray source with an exposure time of 10 s. Because the tube current increased when the tube voltage was increased, the X-ray intensity increased substantially with increasing tube voltage. In this measurement, the intensity rate with a tube voltage of 25 kV was approximately 0.3 μC/kg·s (=10 μJ/kg·s = 10 μGy/s) at 1.0 m from the source.

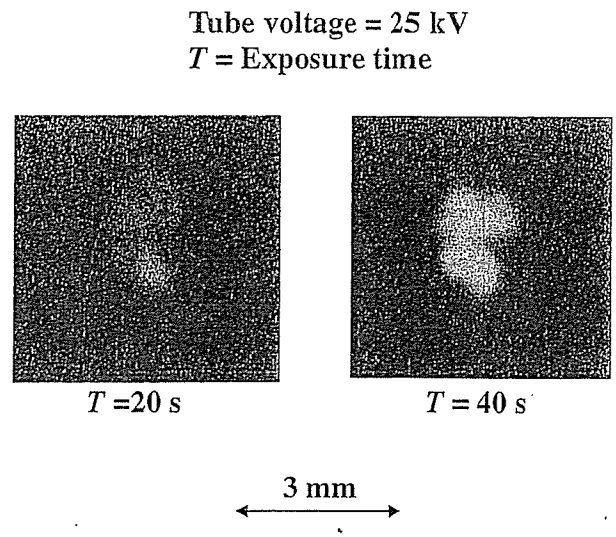

Fig. 4. Images of X-ray source with changes in exposure time.

3.2 X-ray source

In order to measure the images of the X-ray source, we employed a pinhole camera with a hole diameter of 100 μm in conjunction with a Polaroid XR-7 (film). When the exposure time was increased with a tube voltage of 25 kV, the spot intensity increased, but the spot dimensions seldom varied and had values of 2.2 × 1.6 mm (Fig. 4).

3.3 Cathode voltage and tube current

Cathode voltage and tube current were measured using a high-voltage divider and a resistor, respectively (Figs. 5 and 6). In this generator, the cathode voltage is −1 times the tube voltage, and we observed stable cathode voltages. Thereafter, the tube current increased exponentially with increasing tube voltage in a short time. In addition, the current was unstable, and decreased gradually with time.

3.4 X-ray spectra

X-ray spectra were measured using a transmission-type spectrometer with a curved lithium fluoride crystal 0.5 mm thick. The spectra were taken using a computed radiography (CR) system (Konica Regius 150)[17] with a wide dynamic range, and relative X-ray intensity was calculated from Dicom digital data. Figure 7 shows the measured spectra from the transmission-type molybdenum target. We observed lines of characteristic K-series X-rays and K-absorption edges of molybdenum. The characteristic X-ray intensity of the Kα and Kβ lines increased substantially when the tube voltage was increased.

4. Radiography

Radiography was performed using the CR system with a sampling pitch of 87.5 μm. The distance between the X-ray source and the imaging plate was 1.0 m.

Spatial resolution was roughly measured using wires. Radiograms of tungsten wires coiled around a pipe made of polymethyl methacrylate are shown in Fig. 8. Although the

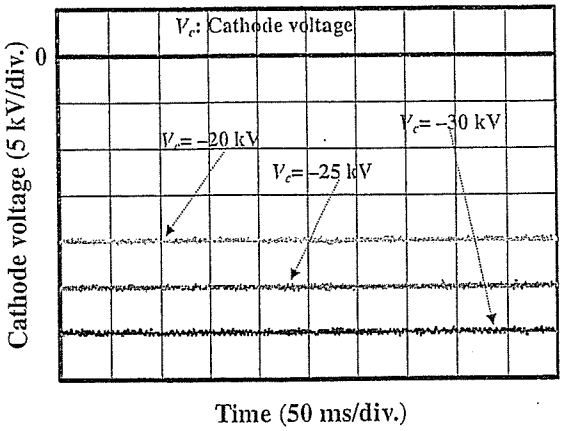

Fig. 5. Cathode voltages.

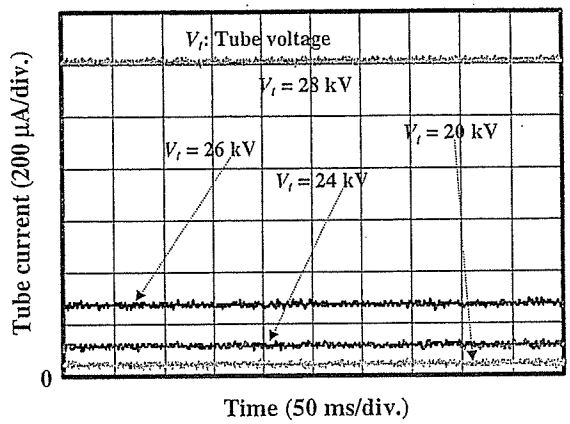

Fig. 6. Tube currents.

image contrast decreased somewhat with decreasing wire diameter due to blurring of the image caused by the sampling pitch, a 50-μm-diameter wire could be observed.

Figures 9 and 10 show angiograms of hearts. Iodine-based microspheres of 15 μm in diameter were used, and coronary arteries and fine blood vessels of approximately 100 μm diameter were visible.

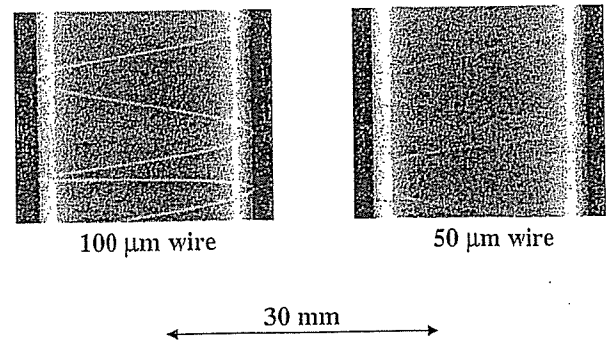

Fig. 8. Radiograms of tungsten wires of 50 and 100 μm diameter coiled around a pipe made of polymethyl methacrylate with tube voltage of 25 kV and exposure time of 20 s.

5. Discussion

In summary, we developed a simple X-ray generator with the cold-cathode diode and succeeded in producing characteristic molybdenum K-series X-rays using the transmission target as the K-edge filter. Subsequently, we confirmed the filtering effect of the target, and bremsstrahlung X-rays with photon energies higher than the edge were rarely detected with a tube voltage of 23 kV.

The current density J (A/cm^2) under field emission is written as:

$$J = 1.54 \times 10^{-6}(V/d)^2 \cdot \exp(-6.8 \times 10^7 \phi^{1.5} d/V)/\phi, \quad (1)$$

where V (V) is the tube voltage, d (cm) is the target-cathode distance, and ϕ (V) is the work function of the cathode element. Therefore, the current values in Fig. 6 corresponded qualitatively to eq. (1).

During the X-ray exposure, although the tube current decreases slightly due to ion sputtering, stable current flow can be obtained by selecting the appropriate cathode material and by controlling the radius of curvature of the cathode tip. In addition, the generator-produced number of

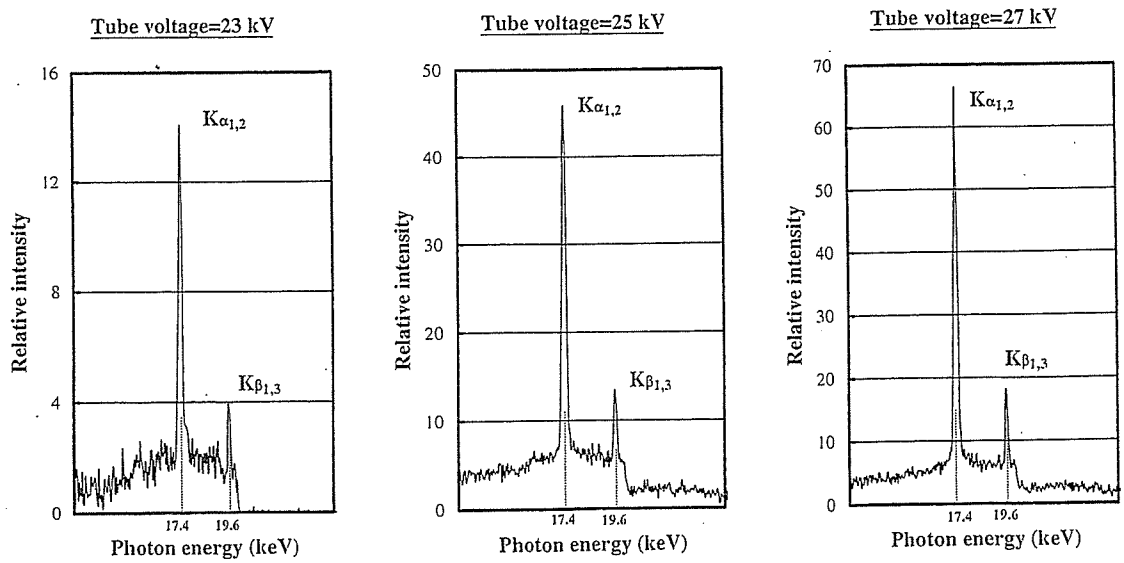

Fig. 7. X-ray spectra.